Bio-based polymer composites obtained by vat photopolymerization of photocurable resins modified with biochar as sustainable filler

Composites: Part A 198 (2025) 109102

Contents lists available at ScienceDirect

Composites Part A

journal homepage: www.elsevier.com/locate/compositesa

Bio-based polymer composites obtained by vat photopolymerization of photocurable resins modified with biochar as sustainable filler

Giovanna Colucci [a,b,*], Federica Di Stefano [a], Francesca Sacchi [a,b], Michela Licciardello [c], Chiara Tonda-Turo [c], Luca Lavagna [a,b], Massimo Messori [a,b]

[a] Politecnico di Torino, Dipartimento di Scienza Applicata e Tecnologia (DISAT), Corso Duca degli Abruzzi 24, 10129 Torino, Italy
[b] National Interuniversity Consortium of Materials Science and Technology (INSTM), Via G. Giusti 9, 50121 Firenze, Italy
[c] Politecnico di Torino, Dipartimento di Ingegneria Meccanica e Aerospaziale (DIMEAS) and PolitoBIOMED Lab, Corso Duca degli Abruzzi 24, 10129 Torino, Italy

HIGHLIGHTS

- Biochar-based polymer composites were prepared via LCD vat-photopolymerization.
- 3D printed parts with complex structures and high level of definition were realized by adding biochar to an AESO resin.
- Thermal, morphological, and mechanical properties were widely studied together with cell viability and cytocompatibility.

GRAPHICAL ABSTRACT

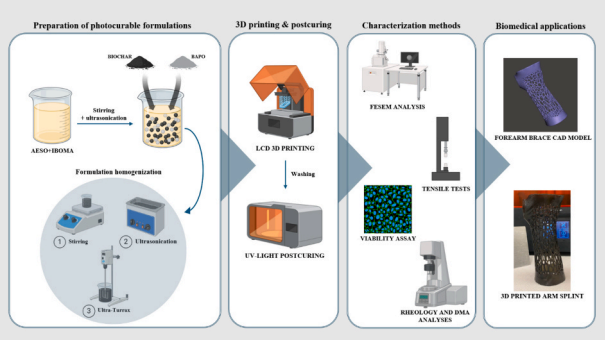

ARTICLE INFO

Keywords:
Biochar
Polymer composites
3D printing
Vat photopolymerization
Liquid crystal display (LCD)

ABSTRACT

The present work focuses on the preparation and characterization of novel bio-based photocured composites realized by vat photopolymerization (VP) 3D printing. Acrylate epoxidized soybean oil (AESO) resin was selected as the monomeric starting material and mixed with isobornyl methacrylate (IBOMA), used as reactive diluent at 50 wt%, in the presence of phenylbis(2,4,6-trimethylbenzoyl) phosphine oxide (BAPO), as radical photoinitiator. The polymerization process was carried out by using a VP technology as the liquid crystal display (LCD) 3D printing. Biochar (BC), deriving from biomass pyrolysis, was added to the resin from 0.5 up to 2 wt% to obtain the final bio-based composites formulations. Rheological measurements were firstly performed to evaluate the viscosity and the printability of the photocurable formulations, and photo-DSC analysis was carried out to study the photo-curing phenomenon and the effects of the BC presence on the curing process within the 3D printer.

After determining the optimal printing parameters, different geometries were printed, leading progressively to the realization of more complex parts with a high number of layers and good dimensional accuracy, such as alternative forearm splints prototypes for biomedical applications. The bio-based composites loaded with biochar underwent several characterization measurements to investigate their thermal, morphological, and mechanical properties. Finally, cell viability and cytocompatibility tests were carried out to study the real applications as bio-based materials for prosthesis development.

* Corresponding author at: Politecnico di Torino, Dipartimento di Scienza Applicata e Tecnologia (DISAT), Corso Duca degli Abruzzi 24, 10129 Torino, Italy.
E-mail address: giovanna.colucci@polito.it (G. Colucci).

https://doi.org/10.1016/j.compositesa.2025.109102
Received 28 March 2025; Received in revised form 16 May 2025; Accepted 7 June 2025
Available online 7 June 2025

1. Introduction

1.1. Biochar

With the new Green Deal, the European Union has been trying to find solutions to waste problems by targeting regulations and reinforcing material reuse and recycling. Although the industries took it upon themselves to try to solve this breach, it remains of high significance within sectors like food, wood, and textile production where the handling and disposal of the wastes remain very challenging. For instance, nearly one-third of food produced for human consumption is wasted, which would work out to about 1.3 billion tons per year [1]. In the case of wood, around 50 million cubic meters of waste are generated each year within the EU [2]. Similarly, a substantial portion of post-consumer waste is neither recycled nor reused, but instead ends up in landfills or undergoes thermochemical treatment for energy recovery [3]. Pyrolysis, a thermochemical treatment method, offers a promising solution for converting biomass waste into energy in the form of bio-fuel (liquid) or syngas (gas) [4–6].

The solid residue produced during this process is biochar (BC), which can vary in size, shape, and chemical properties depending on the feedstock and production methods used [7]. The use of BC in polymer composites has already been studied in the literature [8], primarily to understand its enhancement of both mechanical and electrical properties [9].

Biochar is generally used as a carbon-based additive to enhance the mechanical and electronic performance of polymer composites [10]. It has shown strong potential as a strengthening agent in various polymer matrices [9,11] and also contributes to give improved electrical conductivity [12,13]. These benefits are largely attributed to its high degree of tunability, which depends on the temperature used during its production [14], and its ability to disperse well within polymer matrices [15]. Additionally, biochar surface can be modified with organic or inorganic substances to improve its compatibility and interaction with the polymer matrix [16].

However, the application of BC as a filler in 3D printed polymer composites remains relatively underexplored [17–19].

1.2. 3D printing

There are different 3D printing methods that permit the fabrication of parts and construction of polymer components with very complex structures [20,21]. Among the various additive manufacturing (AM) technologies, vat photopolymerization (VP) is one of the most effective in the production of objects with very high precision and geometrical definition using liquid photopolymers. The light technology achieves very good resolution in printing while accommodating complex shapes [22,23]. In the VP process, a build platform is immersed into the liquid resin, which is cured layer by layer into a solid material using UV light and according to a CAD design. The process is repeated until the object is fully formed [24]. VP technologies are categorized based on the light source employed, including laser-based stereolithography (SLA), direct light processing (DLP), and liquid crystal display (LCD), also known as daylight polymer printing (DPP). The LCD process builds components layer by layer starting from a liquid photocurable resin, selectively curing the thermoset polymer [22,23,25]. In this bottom-up approach, the platform is submerged in the resin, and light emitted from below cures the resin on the platform's surface using an LED lamp integrated with an LCD screen. After each layer is completed, the platform is incrementally raised, and the process continues until the object is finished [26]. Besides, LCD technology provides further advantages, amongst which is a broad range of thermosetting polymers and a platform for the experimentation of other chemistries and reagents. Flexibility makes it easy to customize the photopolymers and their material properties or create new ones. The process makes very good use of cheap raw materials and supports high resolution output in consonance with other sustainable alternatives [27]. However, the larger-scale applications are inhibited by the limited number of eco-friendly photopolymerizable resins [26]. The scientific community has tried to develop sustainable alternatives for current photopolymer print resins that reduce their environmental impact. Recent efforts have focused on developing bio-based, biodegradable and recyclable materials for VP applications e.g., vegetable oils, lignin and saccharides [23,28]. Vegetable oils are the most employed resources for bio-based resins, being characterized by C═C bonds fatty acids, which can be chemically modified with epoxides [29,30], acrylates [31,32], or methacrylates [33], enabling the formation of a thermoset network by UV curing. Moreover, many studies regarding the use of soybean oil in VP have been published. Several research works report the development of soybean oil-based composites obtained by adding a wide range of reinforcements, including calcium silicate, various forms of cellulose, vanillin, as well as powders derived from coconut shells, olive pits, and macadamia nutshells. Additional fillers include titanium dioxide (TiO_2), carbon-based materials, like carbon fibers, carbon nanotubes, and graphene, inorganic compounds, such as silica and alumina, metal powders, and biomass pyrolyzed. However, all the mentioned fillers were incorporated into the same soybean oil-based matrix, but they were processed using VP technology based on Digital Light Processing (DLP) [22,34–41].

Biochar has already been used in 3D printing through several other technologies, including 3D printing of calcified clay concrete for construction applications, extrusion of polypropylene (PP) and high-density polyethylene (HDPE) filaments with biochar as filler, and fabrication of PLA-based composite filaments for Fused Filament Fabrication (FFF) process [19,35,42,43].

Although the literature presents a wide collection of papers on polymer composites 3D printing, the incorporation of biochar as a filler material to soybean oil resin for the realization of composites in VP applications via LCD to the best of our knowledge has not been explored.

Biochar can offer distinct advantages such as high thermal stability and tunable surface chemistry, due to its carbon-rich aromatic structure, can resists to degradation under the heat exposure typical of the curing during an LCD printing. Moreover, its porous structure can help to enhance the dispersion and interfacial adhesion within the photocurable resin. Additionally, BC can contribute to sustainability goals, serving as a carbon-negative additive without compromising printing performance [44].

The novelty of this work lies precisely in the combination between the advantages of the use of biochar as sustainable filler for AESO-based photocurable formulations with the use of LCD as 3D printing VP technology.

This study seeks to merge the benefits of BC-based composites with those of 3D printing. It emphasizes the use of the relatively new LCD technology, which provides superior print quality and accuracy compared to DLP printing [23].

LCD printers also offer larger build volumes assuring less costs than DLP printers, and this makes them more attractive for users who need to print larger and more complex objects without significantly increasing the cost. Moreover, LCD printing process can achieve higher-quality prints with better details due to the uniformity of the light source over the screen, whereas DLP requires more sophisticated and expensive digital projectors.

A glance at the above shows that improvements seem to be due to higher pixel density of the LCD screens, which creates larger components with consistent quality. It must be understood that the LCD 3D printer is business-relatable and cost-effective rather than fast at the expense of DLP printers, gives out a tremendous advantage for a wide range of photocurable resins-spectrum availability and versatility while manufacturing diverse application families, right from prototypes to functional components. Resin viscosity is a critical factor in the LCD process, requiring precise control to ensure optimal flow, layer formation, and curing during printing [45,46].

The incorporation of a bio-derived filler into a 3D printed polymer represents a paradigm event for improving the sustainability of the bio-based polymer composites.

Wu et al. reported in their work the preparation of highly-customized bio-based composites obtained by adding bamboo fibers within a palm oil resin via LCD printing process [47], whereas Colucci et al. 3D printed by LCD bio-based polymer composites filled with agricultural wastes to photocurable acrylate epoxidized soybean oil (AESO) resin [23].

In the present work, novel bio-based composites were prepared by adding spheroidal BC within a photocurable resin such as AESO. 3D printed components were successfully realized by using LCD as VP technology, including some prostheses for possible biomedical applications. The polymeric composites underwent different characterizations from rheological, thermal, morphological, and mechanical point of views. The results of this research reveal that BC can act as filler for the 3D printing of polymeric composite materials, representing effective sustainable and eco-compatible alternatives to conventional ones and fostering a more eco-friendly and environmentally respectful future.

2. Materials and methods

2.1. Materials

Several photocurable liquid formulations were prepared mixing acrylate epoxidized soybean oil (AESO) resin, isobornyl methacryate (IBOMA) as reactive diluent, and phenyl-bis-(2,4,6-trimethylbenzoyl)-phosphine oxide (BAPO) as photoinitiator, all acquired from Merck.

The BC used as filler was provided by a research group from the Politecnico di Torino, which produced it via pyrolysis of crystalline nanocellulose (CNC) at a temperature of 400 °C in nitrogen atmosphere, with a heating rate of 10 °C/min, maintained at the maximum temperature for 30 min.

Human fibroblasts (HFF-1) and human keratinocyte (HaCaT) were obtained from ATCC® and Antibody Research Corporation, respectively. CellTiter-Blue® cell viability assay was purchased from Promega, Milano, Italy. Dulbecco's Modified Eagle's Medium, fetal bovine serum, L-glutamine, penicillin/streptomycin, sodium pyruvate and 4′,6-diamidino-2-phenylindole (DAPI) were purchased from Life Technologies Italy. CellQART® 12-Well transwell inserts were purchased from SABEU GmbH & Co. KG. Paraformaldeide (PFA) was acquired from Alfa Aesar while bovine serum albumin and Triton X-100 were obtained from Merck. Alexa Fluor 488 phalloidin (FITC-labelled) was purchased from BioLegend.

2.2. Photocurable formulations

Several series of photocurable formulations were prepared by mixing IBOMA to an equal quantity of liquid resin (50:50) by magnetic stirring for 2 h at room temperature, in the presence of 2 wt% of BAPO as radical photoinitiator. To obtain a more homogeneous solution and to improve the BAPO dispersion, the formulations were treated using an ultrasonic bath for 15 min at 60 °C, yielding the AESO-based resin.

Among the different bio-based diluents available [24,30], IBOMA was chosen as diluent to reduce the AESO viscosity because of its high reactivity which, combined with the bio-based properties of AESO, offers several key benefits. In fact, IBOMA guarantees superior reactivity, lower viscosity, and better curing efficiency compared to other potential candidates. While other bio-based diluents might provide sustainability, IBOMA is particularly well-suited for photopolymerization process due to its ability to effectively react under UV light, ensuring rapid and complete curing, which is important for high-quality 3D printing. Moreover, IBOMA can help to enhance the mechanical properties by increasing the crosslink density after curing, giving rise to a final material with higher strength crucial for structural applications. The proposed formulation, AESO-IBOMA 50:50, was chosen as a result of a series of experimental tests carried out by preparing mixtures of AESO and different percentages of the IBOMA from 20 up to 50 wt% by analyzing their viscosity and flowability in the 3D printer vat. So that, the bio-based composites were prepared by dispersing different amounts of BC to the AESO-IBOMA formulations. The BC was previously dried in an oven at 100 °C overnight to prevent moisture absorption and then added to the liquid formulation up to 2 wt% using an Ultra-Turrax T 10 basic at 25,000 rpm for 3 min. This step was followed by additional homogenization in an ultrasonic bath at 60 °C for 15 min. Once the BC was homogeneously distributed, the photocurable formulations were stored in a dark environment to prevent premature curing due to light exposure until the printing process occurs.

Multiple sedimentation tests were carried out to assess whether the AESO-filled mixtures can preserve their properties over time by examining the stability of the dispersed BC particles within the AESO-IBOMA resin, which is an important parameter for the further printing process. If the filler tends to precipitate or separates quickly, it indicates a poor dispersion and distribution of BC within the photocurable resin. The sedimentation tests were performed for each BC-filled formulation, providing ongoing observations of the mixture's behavior in the interval range from 1 to 24 h. This can help to choose the geometry of the final parts, which is strongly influenced by both the printing time and the filler content. The black color of BC leads to very dark formulations indicating an acceptable distribution of the filler within the AESO-IBOMA resin up to 8 h, as visible from Fig. 1(a).

Only geometries with a complexity level corresponding to that sedimentation time of the BC were selected for the printing process within the LCD 3D printer. On the contrary, a deposit of BC was noticed at the bottom of the test tube after 24 h of test, indicating a not homogeneous distribution of the BC within the AESO-IBOMA formulation in the presence of concentrations of 1 and 2 wt% of filler, as represented in Fig. 1(b).

2.3. 3D printing of bio-based composites

All the AESO-based formulations were polymerized by using a Phrozen Sonic Mini 8 K VP LCD 3D printer. Exposure time, layer thickness, and speed were set using the Chitubox Software. A comprehensive testing procedure was performed for each formulation to optimize the printing parameters. Initially, the printability of the AESO-based formulation was assessed, starting from printing parameters reported in previous paper on similar resins [24]. Subsequently, a systematic optimization of the relevant settings for the preparation of the photocurable composite formulations was carried out. After printing, the parts were removed from the platform, washed with 2-propanol, left to air-dry for 24 h, and finally post-cured for 1 h under UV light of 405 nm using an Anycubic Wash&Cure Plus machine.

2.4. Characterization methods

The microstructure was studied using a ZEISS Merlin field-emission scanning electron microscope (FE-SEM) produced by Carl Zeiss Microscopy GmbH (Jena, Germany) after metallization with platinum using a Quorum Sputter Coater, model Q150T S (Laughton, East Sussex), for two cycles of 30 s to enhance surface conductivity.

The particle size distribution (PSD) of BC powder was performed by analyzing several thousands of particles using an automated analyzer Morphology 4 (Malvern Panalytical, United Kingdom) to gain a statistical evaluation of the particles size and shape of the filler. It employs a sophisticated image processing software to capture high-resolution images of each particle and to analyze them based on shape features such as diameter, aspect ratio, and circularity.

Thermal properties of the BC and the photocured samples were evaluated by thermogravimetric analysis (TGA) using a Mettler-Toledo TGA 851e Instrument (Columbus, OH, USA), from 25 to 900 °C in flux of air (50 ml min^{-1}) using a heating rate of 10 °C min^{-1}.

The viscosity of the AESO-based formulations was assessed at room

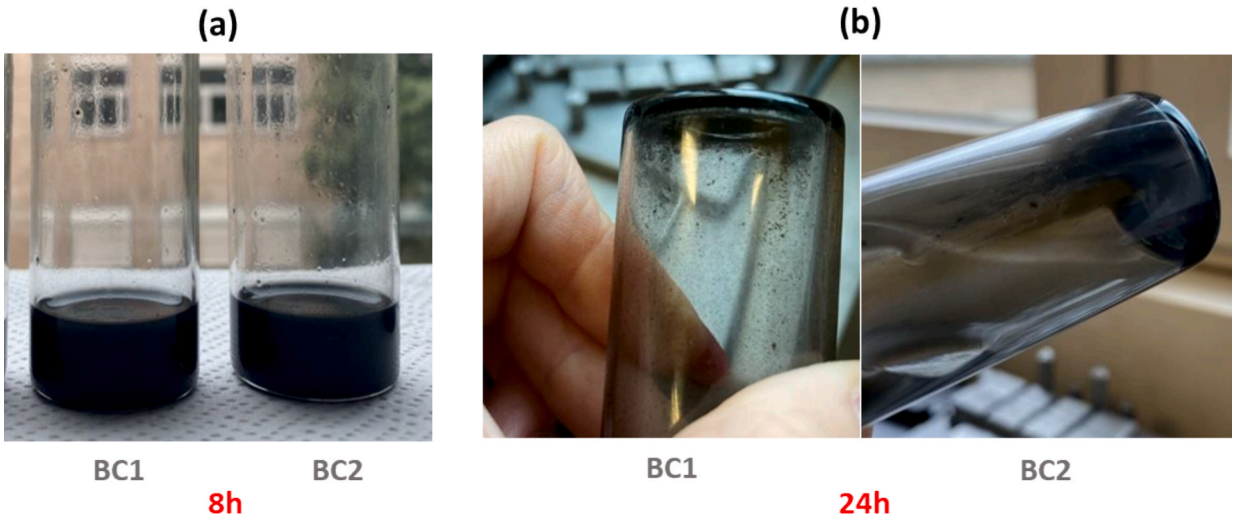

Fig. 1. Sedimentation tests for AESO-IBOMA formulations containing 1 and 2 wt% of BC, after 8 h (a) and 24 h (b). (For interpretation of the references to colour in this figure legend, the reader is referred to the web version of this article.)

temperature using an Anton Paar MCR 702e MultiDrive Rheometer (Graz, Austria) in a parallel plate configuration with a shear range from 0.1 Hz to 1000 Hz.

The photo-curing process was studied using photo-DSC by using a Mettler TOLEDO DSC-1 equipped with a Gas Controller GC100 and an optical fibre characterized by a broad emission spectrum typical of the mercury lamp, Hamamatsu LIGHTINGCURE LC8 (Hamamatsu Photonics. The emission of UV-light was set at 365 nm by using a filter, while the intensity was set at around 100 mW/cm^2. About 8 mg of photocurable formulation was placed in an open aluminium pan (40 μL), whereas an empty pan was used as a reference. The tests were performed at room temperature and in a controlled atmosphere (N_2 flow of 40 mL/min). The samples were irradiated twice in 10 min to properly evaluate the UV-curing reaction. The second run was done to confirm the complete curing and create the baseline. The second curve was subtracted from the first one to obtain the curve related to the curing only. The integration of this curve gives then as result the final conversion (α) of the curing process for each formulation by following Eq. (1):

$$\alpha = \frac{1}{\Delta H_{tot}} \int_t^0 \left(\frac{dH}{dt}\right)_T \quad (1)$$

where ΔH_{tot} is the total enthalpy of the reaction at 100 % crosslinking and dH/dt is the heat flow measured under isothermal condition at 25 °C [48].

The insoluble fraction of the photocured specimens was estimated following the ASTM D2765-84 standard, after 24 h of extraction in chloroform and drying in oven at 80 °C overnight until the weight was constant. The percentage of gel content (G%) reflects the degree of crosslinking of the polymer.

Dynamo mechanical analysis (DMA) was carried out by using an Anton Paar MCR 702e Multi Drive Rheometer (Graz, Austria) in tensile configuration by analyzing printed rectangular specimens with 50 mm of length, 10 mm of width, and 2 mm of thickness and applying uniaxial sinusoidal stress with an amplitude of 1 N and a frequency of 1 Hz in the range of temperature from 0 to 150 °C. Each experiment was terminated once the material reached the rubbery plateau.

From DMA analysis, the crosslinking density of the specimens was also estimated according to the classical rubber theory using Eq. (2):

$$\nu_e = \left(\frac{E'}{3RT}\right) \quad (2)$$

where ν_e is the number of crosslinks per volume of the polymeric crosslinked network, E′ is the storage modulus in the rubbery plateau (Tg + 30 °C), R is the universal gas constant, and T is the temperature in Kelvin [49–51].

Tensile properties were also determined on printed dog-bone specimens (type 5A) according to the standard ISO 527-2, using an Instron 5966 with a 2 kN load cell using pneumatic grips, with a deformation rate of 2 mm min^{-1}.

The cytocompatibility of the AESO-IBOMA reference sample and the composites filled with 0.5, 1, and 2 wt% of BC was evaluated through indirect cytotoxicity test. According to ISO10933-5 guidelines, 0.1f of all samples were incubated in 1 mL of complete HFF-1fibroblasts growth medium (Dulbecco's Modified Eagle's Medium, 15 % fetal bovine serum, 2 % L-glutamine, 1 % penicillin streptomycin) at 37 °C for 24 h, obtaining conditioned medium. HFF1fibroblasts were seeded on 96-well plate at 20 x 10^3 cells/well (n = 6 samples for each condition) and cultured for 24 h in complete medium. The conditioned medium was filtered through a 0.22 μm filter and used to treat HFF-1fibroblasts while control samples (coded as TCP) were obtained by replacing the medium with HFF-1fresh medium. After 24 h, cytotoxicity was evaluated using the CellTiter-Blue® cell viability assay. Briefly, the cell culture medium was removed from each sample and substituted with 100 μL of medium containing CellTiter-Blue® reagent. After 1 h of incubation at 37 °C, 100 μL were placed in a black 96-well plate and cell viability of cells was measured by recording the fluorescent signal using SYNERGYTM HTX multimode plate reader (BioTeK, Winooski, VM, USA) at 530 nm excitation wavelength and 590 nm emission wavelength.

Cell viability was calculated as a percent of the control (TCP). Direct cells contact test was performed to confirm the absence of cytotoxic events when in contact with human skin of AESO-IBOMA sample and the composite loaded with 1 wt% of BC (AESO-IBOMA + 1 % BC), selected as formulation which gave the best results. To this end, human keratinocytes (HaCaT) were seeded on the apical compartment of CellQART® 12-Well transwell inserts at 30 x 10^3 cells/cm^2. The cells were cultured 4 days at liquid–liquid interface, filling apical and basolateral compartment with 0.5 mL and 1 mL, respectively, with complete HaCaT medium (Dulbecco's Modified Eagle's Medium, 15 % fetal bovine serum, 2 % L-glutamine, 1 % penicillin–streptomycin, and 1 % sodium pyruvate). After 4 days, the medium in the apical compartment was removed establishing the culture at air–liquid interface (ALI), to better replicate the properties of human epidermis. AESO-IBOMA and AESO-IBOMA + 1 % BC were punched in circular specimens (0.6 cm in diameter), sterilized with 70 % of ethanol and placed atop the cell layer. Control (CNTR) samples were obtained by leaving the apical compartment just in contact with air. The culture was maintained for additional

7 days.

The viability of HaCaT cells were evaluated by CellTiter-Blue® assay, as previously described. Moreover, the staining of cell nuclei and cytoskeletons was performed to investigate any changes in HaCaT cell morphology resulting from contact with samples. The cellularized transwell inserts were rinsed in phosphate-buffered saline (PBS) and fixed using paraformaldeide 4 % in PBS for 40 min. Then, cells were permeabilized using 0.5 % v/v Triton X-100 for 10 min and blocked in 1 % Bovine Serum Albumin (BSA) for 40 min. The cell cytoskeleton was stained with a solution of Alexa Fluor 488 phalloidin (FITC-labelled) (1:60 dilution in 1 % v/v BSA), while nuclei were stained with DAPI (1:1000 dilution in PBS). After staining, the cells were imaged using Eclipse Ti2 Nikon confocal microscope.

A micro-CT scanner, model Phoenix v|tome|x S240 (GE Baker Hughes-Waygate Technologies, Wunstorf, Germany) was used to inspect one of the 3D printed specimens. The X-ray scanning parameters for the selected 3D printed object were set to a voxel size of 110 μm, 180 kV voltage, 70 μA current, 100 ms exposure time, and 1500 images. The reconstruction of the X-ray image into 3D model was performed using datos|reconstruction software, while VG Studio Max (version 3.4, Volume Graphics, Hexagon Metrology-Volume Graphics, Heidelberg, Germany) was employed for visualization and analysis. Prior to dimensional analysis, surface determination was carried out using the Advanced (classic) approach. This process began with contour identification from the histogram, employing an Automatic material definition at an *iso*-value threshold of 50 %. Based on the results of the surface determination, the nominal/actual comparison analysis module within VG Studio software was applied to evaluate the accuracy of the 3D printed specimen.

3. Results and discussion

3.1. Characterization of biochar

The morphology of the BC powder was evaluated by means of FE-SEM analysis. Fig. 2 shows micrographs of BC at different magnifications: 1 kx (a), 5 kx (b), and 15 kx (c), respectively. The image of Fig. 2 (a) displays the presence of BC spheroidal particles together with few surface defects probably due to the release of volatile organic compounds during pyrolysis. In fact, during the early stages of the thermal degradation for obtaining BC, the surface of the spheres underwent pyrolysis while high-boiling compounds, like levoglucosan, glucose dimers, and trimers, were released from the cores of the particles [52]. As these compounds reached the surface of the powder, they simultaneously started to boil, leading to the formation of small bubbles, clearly visible from Fig. 2(b) at 5 kx, and Fig. 2(c) at 15 kx, respectively. Additionally, the FE-SEM images provide to estimate the BC particles size, which appears in the range from 2 to approximately 6 μm.

Additionally, to better investigate the particle size distribution of BC, a granulometric analysis was carried out by examining thousands of BC particles. Table 1 summarizes the values of the particles size distribution, aspect ratio, and circularity of the spheroidal BC evaluated by morphological imaging.

The results suggest that the BC filler particles have an average diameter of 5.5 μm and circularity close to 0.97 confirming the indication of the previous FESEM analysis.

Fig. 3 reports the TG curve and the first derivative curve of the spheroidal BC powder. The initial weight loss can be seen in the region of 100–120 °C and it is attributed to the evaporation of the moisture absorbed on the BC particles surface. The experimental results indicate that there is a weight loss of 5 % at around 323 °C.

The BC thermal degradation occurs in three main steps, with the first degradation peak at 378 °C, followed by a second peak at 421 °C where the sample has lost half of its weight, and a final peak at 523 °C, suggesting that BC has lost 90 % of its weight. This significant volatile release can be assigned to the thermal decomposition of the three main

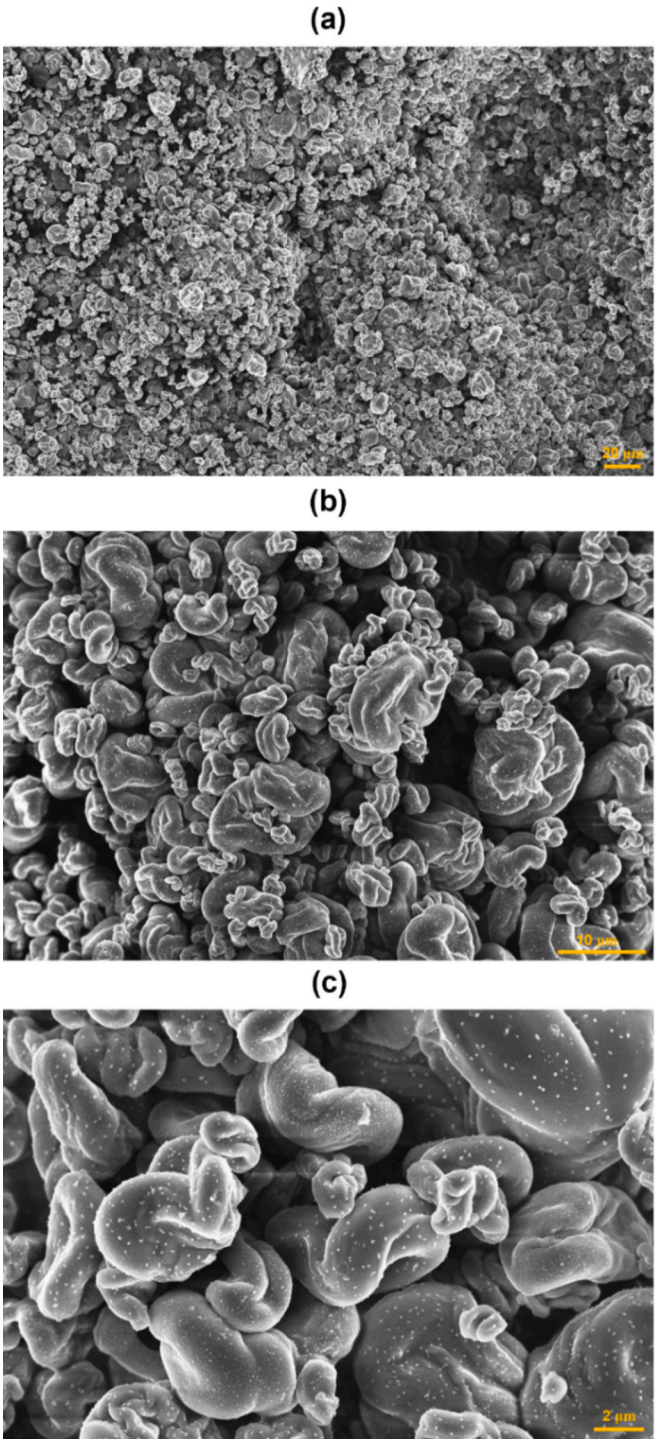

Fig. 2. FE-SEM micrographs of spheroidal BC at different magnifications: 1 kx (a), 5 kx (b), and 15 kx (c). (For interpretation of the references to colour in this figure legend, the reader is referred to the web version of this article.)

Table 1
BC diameter, aspect ratio, and circularity evaluated by morphological analysis.

Sample code	Diameter (μm)	Aspect ratio	Circularity
BC	D [n, 0.1]: 1.9 D [n, 0.5]: 4.4 D [n, 0.9]: 10.3	D [n, 0.1]: 0.52 D [n, 0.5]: 0.74 D [n, 0.9]: 0.90	D [n, 0.1]: 0.76 D [n, 0.5]: 0.91 D [n, 0.9]: 0.97

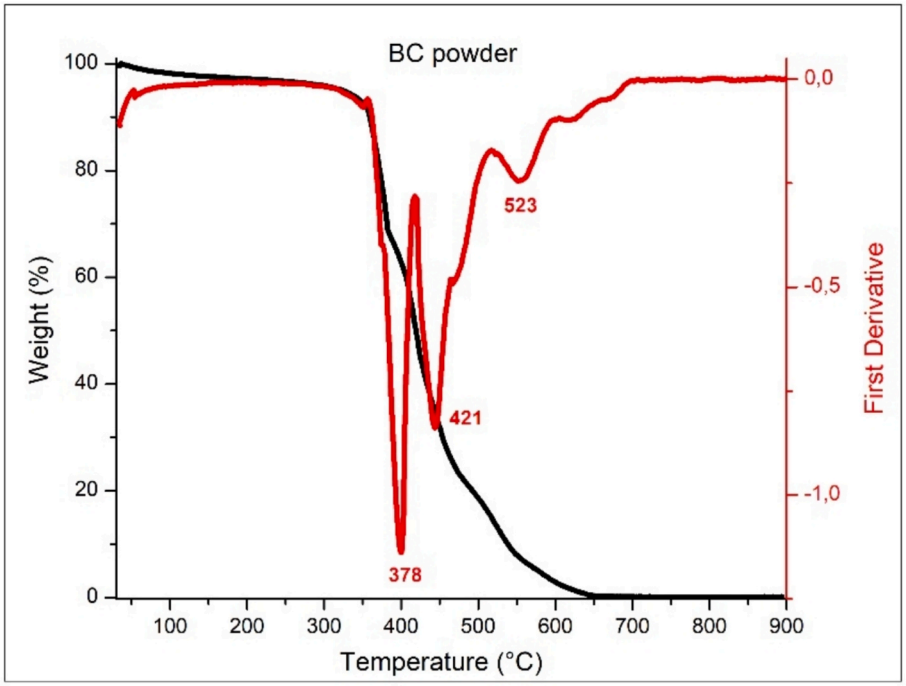

Fig. 3. TG curve (black) performed in air and DTG (red) curve of the BC powder. (For interpretation of the references to color in this figure legend, the reader is referred to the web version of this article.)

BC constituents, namely: hemicellulose, cellulose, and lignin [53]. No ash remains at the end of the analysis performed in air at 900 °C, indicating the absence of inorganic residues. This result can be explained considering that the cellulose employed to prepare the BC did not contain inorganic components in its own chemical composition. Furthermore, this result also highlights that the pyrolysis process was optimally conducted, and no impurities were present in the final synthesized BC powder.

3.2. Rheological assessment of AESO-based photocurable formulations

In the context of VP process, including LCD-based 3D printing, the viscosity plays a crucial role in the success of printing process, affecting the flow characteristics. The addition of a reactive diluent to the photopolymer resin help to significantly reduce viscosity and ultimately impact its printability. For this reason, IBOMA was added as reactive diluent within the photocurable resin. To identify a suitable base formulation, several photocurable mixtures were prepared by mixing AESO with different weight ratios of IBOMA in a range between 20 and 50 wt%, in the presence of BAPO as photoinitiator for each formulation. Then, their viscosities were measured at 25 °C and a shear rate of 10 s^{-1}. The results obtained show that the formulations containing lower amounts of diluent have values of zero-shear viscosity of 2784 cP for AESO-IBOMA 80:20 and 1158 cP for AESO-IBOMA 70:30, respectively. These viscosities are significantly higher than the limit of 1000 cP for ideal 3D printing processes via VP, as reported in literature [24,54]. On the contrary, the formulations AESO-IBOMA 60:40 and AESO-IBOMA 50:50 meet the viscosity requirement showing values in the acceptable range, 554 cP and 365 cP, respectively. However, considering that the addition of biochar as filler was expected to further increase the resin viscosity, AESO-based mixtures containing 50 wt% of AESO and 50 wt% of IBOMA were selected as the best formulation in terms of viscosity and processability even after biochar incorporation and employed as reference system. So therefore, BC was dispersed within the liquid formulations at different concentrations, from 0.5 up to 2 wt%. The effect of the BC addition on the resin viscosity and flowability was studied considering their key role for a VP 3D printing process [24]. This is because during a printing process via LCD high viscosity values lead to longer printing times and lower rates [26].

Table 2 shows the viscosity values at room temperature of the AESO-IBOMA reference system, and the values of the bio-based composites obtained by adding different amounts of BC.

It is noteworthy that, although viscosity values increase with the BC content, the optimization of the formulation's composition ensures that the viscosity remains below the ideal range for VP technologies, as reported in literature [24,54,55]. This indicates that higher filler content can be still feasible.

Photo-DSC were also performed on the photocurable formulations to study the photo-curing process behavior. Photo-DSC analysis allows for the evaluation of the influence of BC on the reactivity of the AESO-IBOMA photopolymerizable system, through three main parameters: h_{peak}, ΔHexp, and t_{peak}. The h_{peak} parameter represents the maximum heat release rate during the photoinduced reaction and it is proportional to the maximum polymerization rate. ΔH_{exp} indicates the total enthalpy released during the process, reflecting the overall conversion degree. The t_{peak} parameter, instead, indicates the moment at which the maximum peak of the exothermic reaction occurs [48,51].

Fig. 4 reports the photo-DSC curves of the AESO-based photocurable formulations unfilled and filled with BC. The measured heat flow is assumed to occur solely due to one reaction, the crosslinking of the

Table 2
Rheological properties and kinetics conversion of AESO-based photocurable formulations.

Sample code	BC content (wt. %)	Viscosity[a] (mPa s)	Conversion[b] (%)
AESO-IBOMA	0	365	100
AESO-IBOMA + BC0.5	0.5	412	99
AESO-IBOMA + BC1	1.0	433	98
AESO-IBOMA + BC2	2.0	461	95

[a] Zero-shear viscosity (η_0) evaluated at 25 °C at a shear rate of 10 1/s.
[b] Kinetics conversion of the photocurable formulations obtained following Eq. (1) after 120 s.

acrylate groups present in the AESO matrix structure.

From Fig. 4(a), it can be observed that the increase in BC content determines a progressive reduction of both the reaction rate h_{peak} and the total enthalpy released ΔH_{exp}, suggesting that BC has an inhibitory effect on the photopolymerization process, limiting both the intensity and the overall effectiveness of the reaction. This behavior can be due to the absorption or reflection of part of the UV light due to the black coloration of the filler, which inhibits and reduces the photopolymerization through a physical barrier effect that limits the molecular chains' mobility and the diffusion of radicals in the matrix [48].

Another interesting finding concerns t_{peak}, which tends to slightly anticipate by increasing the biochar content. This could indicate a greater initial activation of the material surface, due to local optical phenomena such as light diffusion, but does not imply greater efficiency of the reaction. On the contrary, the anticipation of the peak is followed by a decrease in the overall reaction, as confirmed by the reduction of h_{peak} and ΔH_{peak}.

The addition of BC has a negative effect on the kinetics of the reaction and extent of photoinduced crosslinking, significantly reducing the maximum reaction rate and the conversion, as visible from Fig. 4(b). The degree of conversion shifts from 100 % for the unfilled AESO-IBOMA formulation up to 95 % of conversion for the biochar-based composites, as evidenced by the data reported in Table 2. This effect is evident at all concentrations of BC, but it is much more marked in the presence of 2 wt% of BC, where there is a reduction in the released enthalpy of about 30 % compared to the reference unfilled sample. The kinetics of conversion as a function of time of the photocuring process for the AESO-based formulations filled with BC decrease from 99 % up to 95 %. This result suggests that the use of BC in photopolymerizable systems requires careful optimization of the formulations preparation and the optimization of the printing parameters.

3.3. 3D printing process of complex structures

Based on the photo-DSC results, different printing tests were first carried out to assess the effective printing parameters and the printability of the AESO-based resins by LCD. The best printing parameters for each formulation were listed in detail in Table 3.

In addition to the simple geometries, rectangular and dog bone-shape necessary for the characterization tests, a variety of complex objects were successfully 3D printed, showing an excellent resolution and dimensional accuracy with both reference AESO-IBOMA system and the composite formulations containing increasing BC content, as shown from the pictures of Fig. 5. Firstly, a small vase composed of 350 layers, and standing at 35 mm in height, was printed using the unfilled photocurable AESO-based formulation, as visible in Fig. 5(a). This part features a complex diagonal grid-like structure, characterized by a series of intersecting lines that create a dynamic pattern of openings throughout its surface. Notably, the part exhibits a variable diameter that changes with the whole height.

Moreover, a helicoidal complex of 450 layers and 45 mm in height was printed showing an intricate curvatures and smooth, continuous spirals, demonstrating the printer's capability to realize complex geometries with high level of definition, as visible from the picture of Fig. 5 (b).

The same vase objects were then printed via LCD using the AESO-based formulations containing different amounts of BC to ensure the replicability of the filled resin, even in different size and with different internal patterns, as shown in Fig. 5(c) for a composite containing 1 wt% of BC. The component, illustrated in Fig. 5(d), is like the previous one but it presents a different structural complexity, very challenging to print. Although, it maintains the same external shape, it shows a

Table 3
LCD printing parameters for AESO-based photocurable formulations.

	AESO-IBOMA	AESO-IBOMA + BC0.5	AESO-IBOMA + BC1	AESO-IBOMA + BC2
Layer height (mm)	0.1	0.1	0.1	0.1
Exposure time (s)	15	18	22	40
Bottom exposure time (s)	18	20	30	45
Rest time before lift (s)	0	0	0	0
Rest time after lift (s)	0	0	0	0
Rest time after retract (s)	4	4	4	4
Lifting distance (mm)	4	4	4	4
Retract distance (mm)	6	8	8	8
Lifting speed (mm/min)	80	80	80	80
Retract speed (mm/min)	80	80	160	160

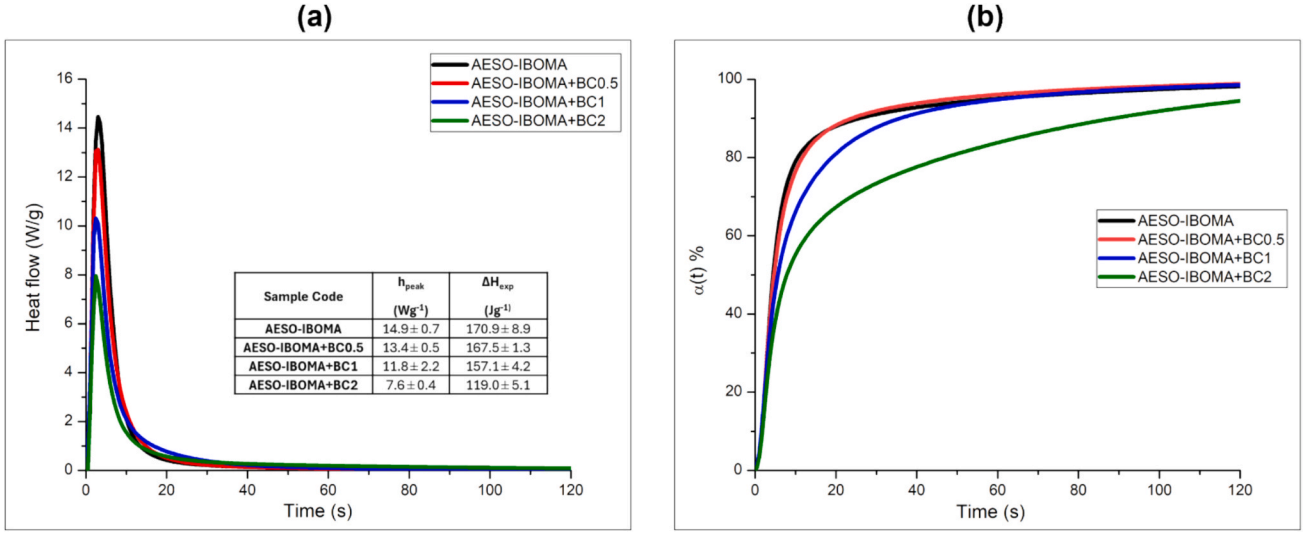

Fig. 4. Photo-DSC (a) and kinetics (b) curves of the photocurable formulations unfilled and filled with BC. (For interpretation of the references to colour in this figure legend, the reader is referred to the web version of this article.)

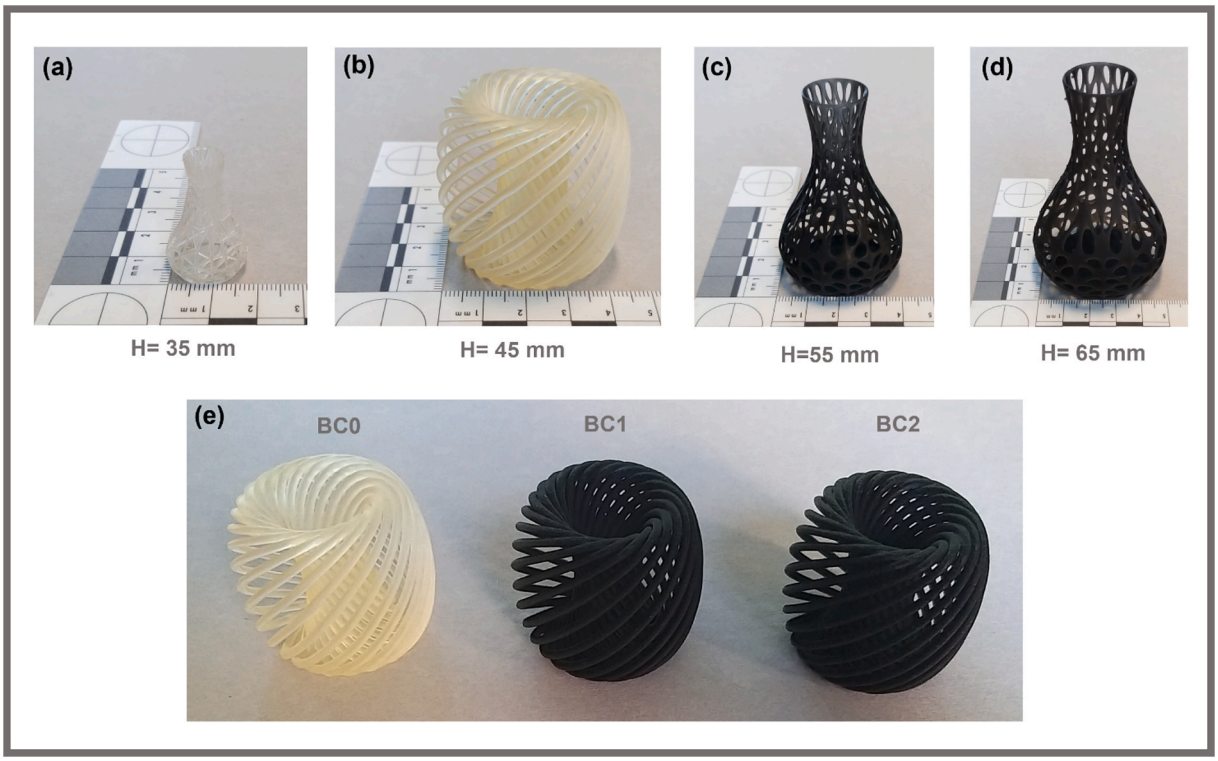

Fig. 5. 3D printed AESO-based objects unfilled (a,b) and filled with different amounts of BC (c,d,e). (For interpretation of the references to colour in this figure legend, the reader is referred to the web version of this article.)

distinctive texture. Instead of a diagonal grid pattern, it evidences a continuous mesh with holes of varying sizes, depending on the height position. These last two designs resemble the patterns found in literature for 3D printed splints for forearms, which can represent valid alternatives to the traditional casts for biomedical applications.

Overall, all the printed structures reveal an optimal print quality, confirming the effectiveness of the composite materials in achieving precise geometric fidelity even in the presence of the filler. The helical complex maintains its intricate geometry across the different formulations, underlining the ability of the BC-loaded formulations to realize complex structures ensuring the structural integrity up to composites filled with 2 wt% of BC, as shown in the pictures of Fig. 5(e).

The parameters set for the printing process of the AESO-based formulations are optimally chosen, resulting in good dimensional accuracy, even with the inclusion of a dark filler, like BC, which could strictly influence the success of the printing process.

3.4. Gel content

The gel content of the printed AESO-based samples shows values higher than 99 % for all the systems investigated, as reported in Table 4. The results put in evidence that the addition of the filler does not substantially affect the material's crosslinking degree despite the black color of the BC interferes with the photopolymerization process by absorbing UV light.

Moreover, the values reveal that the printing parameters were optimized for ensuring high conversion of the monomers into the 3D printer.

3.5. Morphology of bio-based composites

A morphological analysis was carried out by FE-SEM on the fracture surfaces of the unfilled AESO-IBOMA specimens, used as reference, and on those of the bio-based composites filled with different percentages of BC, as reported in Fig. 6.

From the images of Fig. 6(a) acquired at 5 kx of magnification, it is possible to see how the fracture surface of the unfilled photocured system appears smooth and homogeneous since no filler has been incorporated within the resin. In fact, no signs of irregularities or defects are visible.

The fracture surface of the sample containing 1 wt% of BC, observed at a magnification of 5 kx, shows that the filler is uniformly distributed throughout the polymer matrix.

The sample exhibits the presence of nearly spherical particles

Table 4
Gel content, thermal, and viscoelastic properties of bio-based samples.

Sample code	G[a] (%)	T_{onset}[b] (°C)	$T_{max\ deg}$[c] (°C)	E′[d] (MPa)	E″[d] (MPa)	$T_{tan\delta max}$[d] (°C)	ν_c[e] (mol/m^3)
AESO-IBOMA	99.7	279	317/401/558	1140	117	93	1,03E+03
AESO-IBOMA + BC0.5	99.6	264	318/404/557	1186	133	92	1,36E+03
AESO-IBOMA + BC1	99.6	261	319/405/554	1315	113	86	1,26E+03
AESO-IBOMA + BC2	99.7	251	320/408/550	984	104	81	1,09E+03

[a] Gel content percentage (G%) determined after 24 h in chloroform.
[b] Onset temperature (T_{onset}) determined by TGA.
[c] Maximum degradation temperature determined by DTG curves.
[d] Storage modulus (E′), loss modulus (E″), and maximum of tan delta curves ($T_{tan\delta max}$) determined by DMA.
[e] Crosslinking density determined by DMA analysis in the rubbery region (303 K) by using Eq. (2).

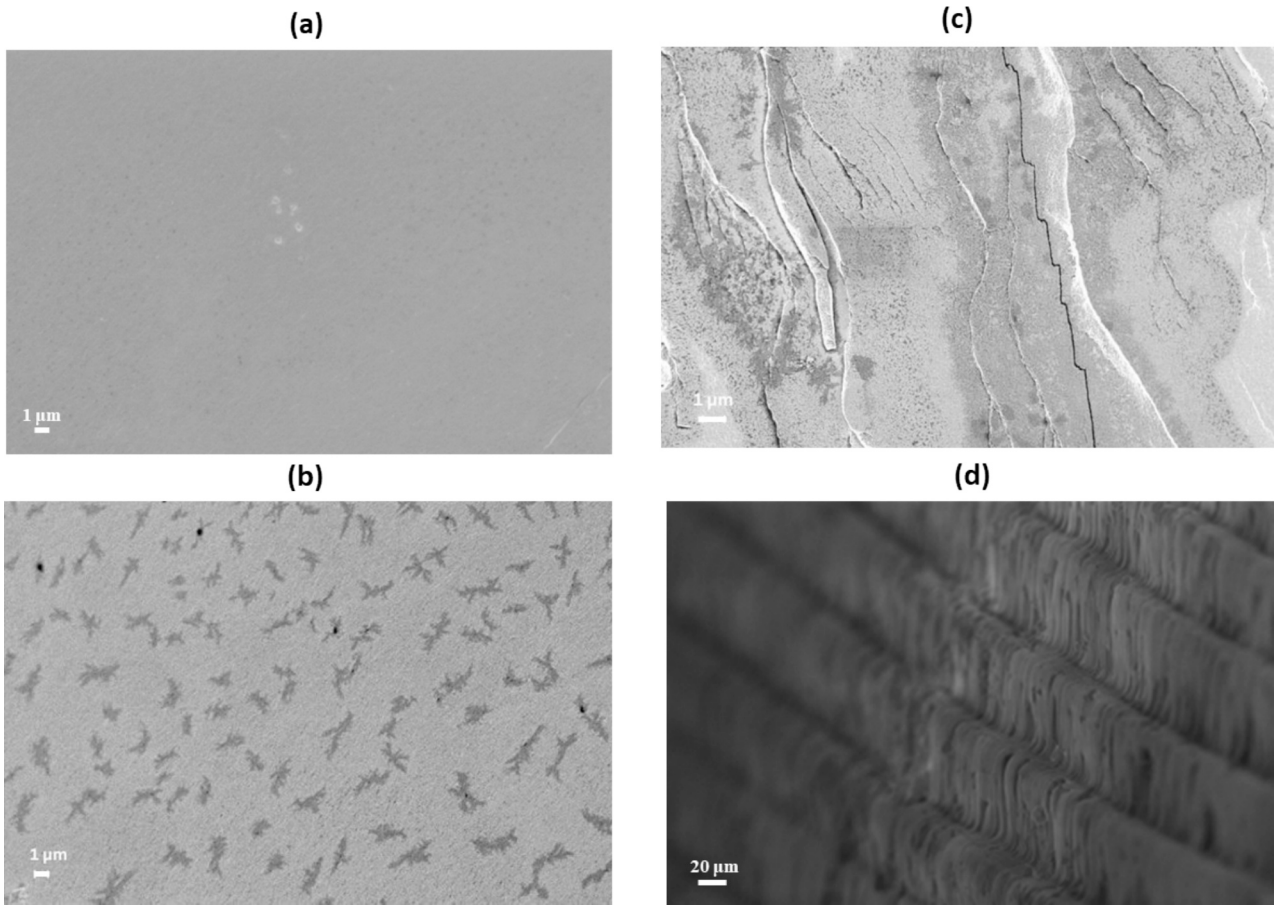

Fig. 6. FE-SEM images of the fracture surface of 3D printed AESO-THFA unfilled (a) and filled with 1 wt% (b) and 2 wt% (c) of BC. Micrograph showing the layer-by-layer structure formed during the printing process (d).

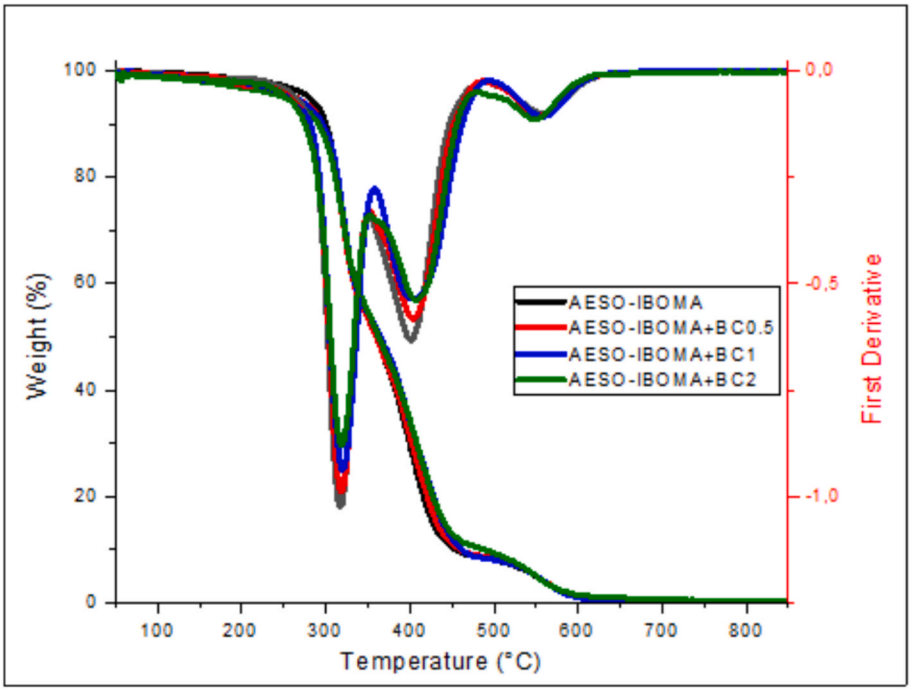

Fig. 7. TG and DTG curves of 3D printed samples unfilled or filled with BC. (For interpretation of the references to colour in this figure legend, the reader is referred to the web version of this article.)

embedded within the matrix, which is no longer smooth and homogeneous, due to the spherical-like geometry of the BC, as visible from Fig. 6 (b).

A completely different morphology was observed in Fig. 6(c) for the specimen with the highest amount of BC powder (2 wt%). The FE-SEM micrograph at 5 kx evidence that BC is not well-dispersed within the polymer matrix. It appears to be clustered around the fracture surface of the sample. This behavior lets to conclude that further analyses are necessary for better dispersing the BC within the resin and assessing the final mechanical properties of the composites.

Furthermore, Fig. 6(d) illustrates the good layer-by-layer deposition of the AESO-based formulation filled with 1 wt% of BC occurring during the printing process within the vat. This finding underlines that the selected printing parameters are useful for ideal LCD processing.

3.6. Thermal and viscoelastic properties of bio-based composites

The thermal stability of the bio-based 3D printed samples was evaluated by means of TGA.

The TG and DTG curves of the AESO-IBOMA reference sample and of the composites loaded with 0.5, 1, and 2 wt% of BC are shown in Fig. 7.

By analysing the thermograms, it is noticeable that, compared to the unfilled reference specimens, those containing BC powder show a slight decrease of the onset temperatures as the BC content increases, shifting from 279 °C for the AESO-IBOMA resin to 251 °C for the specimens containing 2 wt% of BC, as summarized from the data of Table 4.

This trend can be explained considering that the initial weight loss is usually due to the elimination of moisture or the release of volatile compounds. Since the BC filler comes from cellulose pyrolysis, it introduces a certain internal porosity into the resin which can retain more moisture, leading to greater weight loss at lower temperature stages [14].

At higher temperatures, the maximum degradation peaks occur almost at the same temperature, indicating that once moisture is removed from the samples, the presence of different amounts of BC does not affect the final thermal stability of the photocured systems.

Furthermore, the ash content values at the end of each analysis, at 900 °C, are zero for all specimens since both the BC and the resin formulations are organic materials without any other inorganic residues. This also confirms that no inorganic contamination occurred during the formulation's preparation nor during the printing process.

DMA tests were also performed for each formulation to evaluate the viscoelastic properties of the 3D printed unfilled and filled samples. Fig. 8 displays the storage modulus (a), the loss modulus (b) and the extensional loss factor values (c), respectively.

Looking at the comparison between the curves of the storage and loss moduli, a clear trend can be observed. In fact, the storage and loss modulus values decrease with increasing temperature, indicating a reduction in both energy dissipation and elastic energy storage, as evident in Fig. 8(a) and (b). This is a specific characteristic of the thermosetting polymers as they shift from a glassy to a rubber state depending on the temperature. The temperature at which this transition occurs, marked by the maximum of the tan delta curve as a function of the temperature, corresponds to the glass transition temperature (T_g). The representative values from the analysis detected at 25 °C are summarized in Table 4. The data shows that the storage modulus (E') increases by adding the BC from 1140 MPa for the unfilled system to 1315 MPa for the composites containing 1 wt% of BC powder. By increasing the amount of BC up to 2 wt%, it is evident a significant decrease of the modulus to suggest that if the BC initially improves the mechanical performance of the system, at higher concentrations the effect declines, probably due to the clustering of BC particles, as already observed in the FESEM analysis at this concentration. These clusters can disrupt the effective dispersion of the filler within the polymeric resin resulting in a reduction in overall mechanical performance. At the same time, the loss moduli slight increase in the presence of lower amount of BC (0.5 wt%) from 117 to 133 MPa, but the values decrease by increasing the BC content up to 2 wt% reaching a value of 104 MPa.

The DMA results show that the storage modulus is consistently higher than the loss modulus across all the specimens, leading to a tan delta value of less than one, which indicates a predominantly elastic behavior of the materials. The T_g values slightly decrease by increasing the BC content from 93 °C for the unfilled system to 81 °C for the composites loaded with 2 wt% of BC. The tan delta curves profiles, reported in Fig. 8(c), suggest that the tested samples show transitions more readily from the glassy state to the rubbery state as more filler is incorporated. This result can be explained by considering a slight increase of the polymeric chains' mobility induced to the BC particles within the polymer matrix.

From DMA analysis was also possible to estimate the crosslinking density of the AESO-based composites following Eq. (2) by measuring the storage modulus in the rubbery plateau, well above the Tg of the polymer, according to the classical rubber theory equation [50].

Here the crosslinking density was calculated at 30 °C (303 K), well above the glass transition temperature of the unfilled and filled AESO-based samples. It is interesting to note that there is a slight increase of the crosslinking density in the presence of increasing amount of BC up to 1 wt%. However, for higher BC content (2 wt%) the crosslinking density decreases following the same trend of the storage modulus confirming that the BC particles tend to form aggregates negatively affecting the curing process and, therefore, the mechanical performance, as already discussed. These observations are further supported by the results of tensile testing.

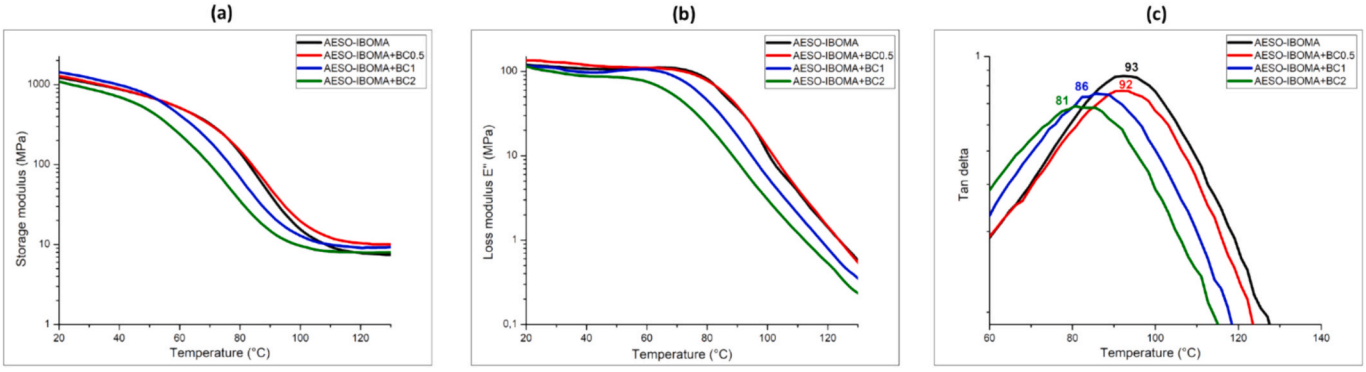

Fig. 8. DMA curves of printed samples unfilled and filled with BC corresponding to the storage modulus (a), loss modulus (b) and the tan delta values (c). (For interpretation of the references to colour in this figure legend, the reader is referred to the web version of this article.)

Table 5
Tensile properties of AESO-based samples unfilled and filled with BC.

Sample code	Young's modulus (MPa)	Ultimate tensile strength (MPa)	Elongation at break (%)
AESO-IBOMA	634 ± 42	29 ± 1	7.5 ± 1.0
AESO-IBOMA + BC0.5	643 ± 39	24 ± 1	7.0 ± 1.0
AESO-IBOMA + BC1	679 ± 40	22 ± 1	7.0 ± 1.0
AESO-IBOMA + BC2	517 ± 18	19 ± 1	7.0 ± 1.5

3.7. Tensile testing of bio-based composites

Tensile measurements were carried out to highlight the main trends in the mechanical properties of the different formulations, focusing on the elastic modulus, the ultimate tensile strength, and the elongation at break percentage. The key data of tensile tests are listed in Table 5.

The introduction of BC slightly increases the stiffness of the polymer. The Young's modulus rises from 634 MPa for the unfilled resin to 679 MPa for the formulation with 1 wt% of BC, indicating that small amounts of powder can enhance the rigidity of the AESO-IBOMA material.

However, when the BC content reaches 2 wt%, the elastic modulus value significantly decreases to 517 MPa. This result suggests once again that a higher filler amount can lead to a reduction of the stiffness of the AESO-based polymeric system, surely caused by the BC particles aggregation, as already seen from FE-SEM analysis, or by their inadequate dispersion in line with the earlier DMA findings. Tensile strength also decreases as the filler content increases. For the unfilled printed specimens, the ultimate tensile strength is 29 MPa, which drops up to 19 MPa by increasing the BC content. Similarly, the elongation at break also slightly decreases by increasing the amount of BC powder. This suggests that the addition of filler reduces the polymer's ductility. To conclude, the addition of BC up to 2 wt% enhances the stiffness of the material, as indicated by the increased elastic modulus. However, this enhancement is accompanied by a decrease in both the ultimate tensile strength. The elongation at break percentage remains almost the same. As the BC content increases a significant decline in mechanical properties occurs, revealing a decrease in the elastic modulus and the tensile strength. This finding suggests that there is a clear threshold for BC incorporation, beyond which its presence can negatively impact the material final mechanical performances.

Based on the collected data, the formulation with 1 wt% of BC is considered optimal as it ensures a good balance between improved stiffness, acceptable tensile strength, and proper filler dispersion, as already confirmed by FESEM analysis. At this concentration, the material maintains good printability and avoids the aggregation issues observed at higher loadings. For these reasons, this concentration was selected to characterize the material with in vitro cell tests to evaluate its cytocompatibility.

3.8. In vitro cell tests

The cytocompatibility of the samples was evaluated through indirect cytotoxicity tests by culturing HFF-1 fibroblasts with complete medium previously conditioned with the different formulations for 24 h [56]. The result of cytotoxicity tests was reported in Fig. 9. No statistical differences in cell viability were detected in the case of unfilled and filled BC-based composites compared to control (TCP) demonstrating the cytocompatibility of specimens.

Finally, direct cell contact tests were performed to confirm the potential use of AESO-IBOMA sample and AESO-IBOMA + BC1 as biomaterials to produce prosthesis such as forearm splints. To this end, the viability (Fig. 9) and morphology (Fig. 10) of HaCaT keratinocyte cultured in contact with AESO-IBOMA sample and AESO-IBOMA + BC1 was evaluated and compared to cells cultured in the apical side of transwell insert without any sample in contact (CNTR). As shown in Fig. 9, a high cell viability was recorded in all the samples confirming the biocompatibility of specimens.

Moreover, the fluorescence staining (Fig. 10), showed the presence of a uniform layer of spread HaCaT keratinocyte which maintained their typical polygonal shape in all the samples.

These results demonstrate that the presence of unfilled and filled BC-based samples does not affect the cell viability and morphology.

Considering the good results of the cell viability and

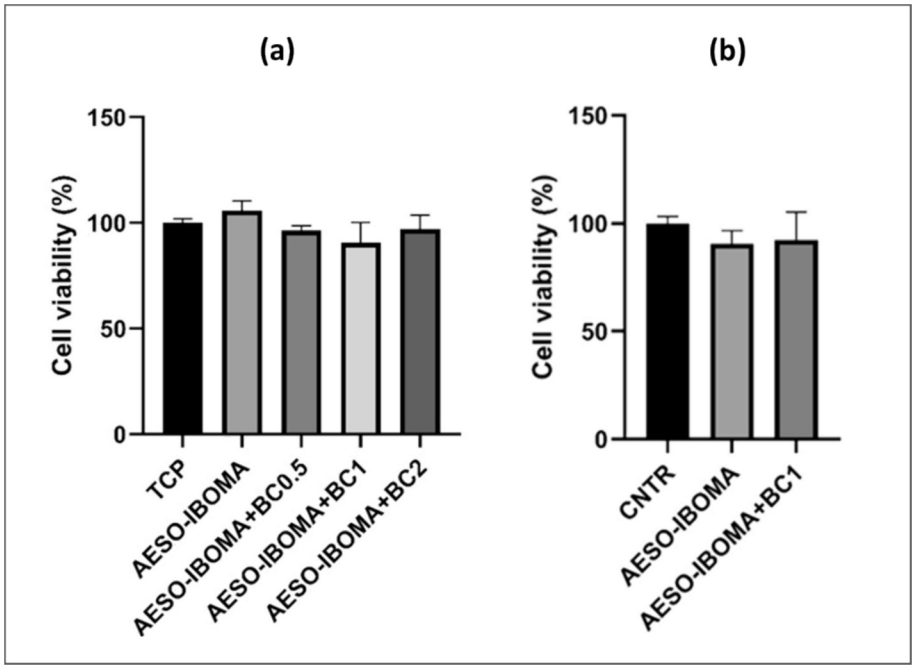

Fig. 9. Evaluation of cell viability through CellTiter-Blue® assay after 24 h of HFF-1 fibroblast culture with sample extracts (a) and of HaCaT keratinocyte cultured in contact with AESO-IBOMA and AESO-IBOMA + BC1 specimens for 7 days (b).

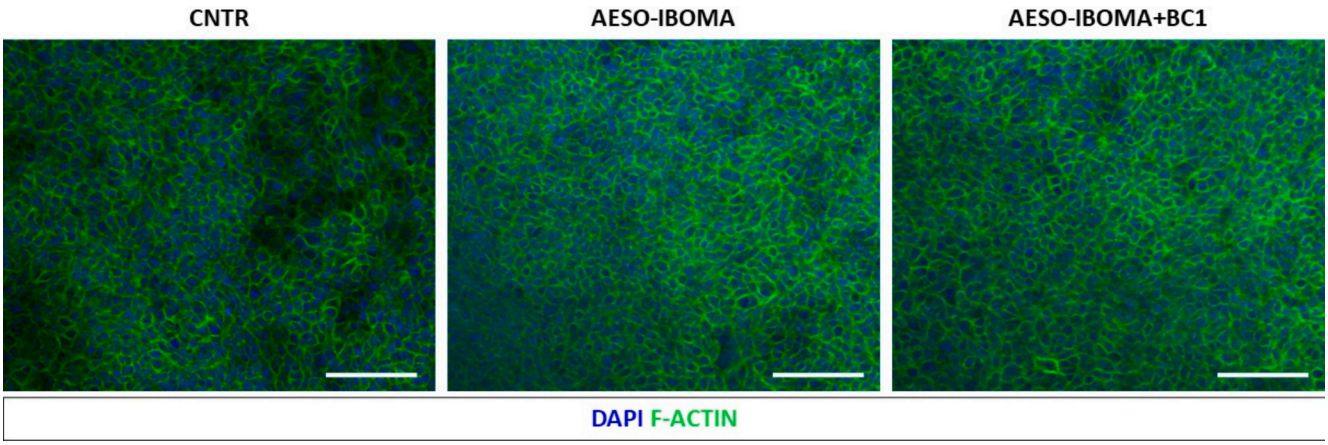

Fig. 10. Representative fluorescence images of HaCaT keratinocyte cultured on the membrane of the traswell insert (CNTR), in contact with AESO-IBOMA and AESO-IBOMA + 1 % BC specimens for 7 days. Scale bar = 100 μm. (For interpretation of the references to colour in this figure legend, the reader is referred to the web version of this article.)

cytocompatibility tests, two different complex structures were 3D printed for applications in the biomedical sector, such as bio-based alternatives forearm splints realized using the best formulation, containing 1 wt% of BC.

Fig. 11 presents some pictures relative to the unfilled (a) and BC-based (b) specimens obtained by VP LCD. Two different arm brace prototypes were successfully 3D printed as innovative alternatives to the traditional plaster braces for patients with a broken forearm. The first unfilled prototype can fully cover the forearm of the patient and was produced by the deposition of 1100 layers of AESO-based formulation as visible from Fig. 11(a). The second model consisting of 1400 layers (14 cm) was realized by adding 1 wt% of BC within the photocurable formulation and represents a prototype which covers only the upper part of the human forearm as reported in Fig. 11(b), providing more flexibility based on the severity and location of the injury. The same objects were reported from different points of view in the other pictures of Fig. 10: top view (c), bottom view (d), and side view (e). Both models feature an aesthetic and functional perforated design, more challenging to print, that enhance the ventilation, reducing the risk of sweating, allergic reactions, and skin irritation [57]. The holes in the texture of the two different architectures also allow the affected area to be washed, promoting better hygiene during the recovery process, as clearly shown from the different angles in Fig. 11(c), (d), and (e).

An opening for the patient's thumb is incorporated in both models, ensuring stability and a proper positioning, keeping the brace securely in situ during use. Moreover, the open structure permits for visual monitoring of the injured area, enabling doctors to inspect the injury without removing the brace, thus aiding in accurate diagnoses during follow-up visits [58].

Additionally, both the 3D printed forearm splints are significantly lighter than traditional plaster casts, improving comfort and mobility for the patient. These innovative prototypes demonstrate the potential of 3D printing to provide personalized, breathable, and hygienic solutions that can help to enhance the recovery experience of the patient.

To conclude the study, the 3D printing accuracy of the most complex specimen filled with BC, the forearm splint model was assessed using

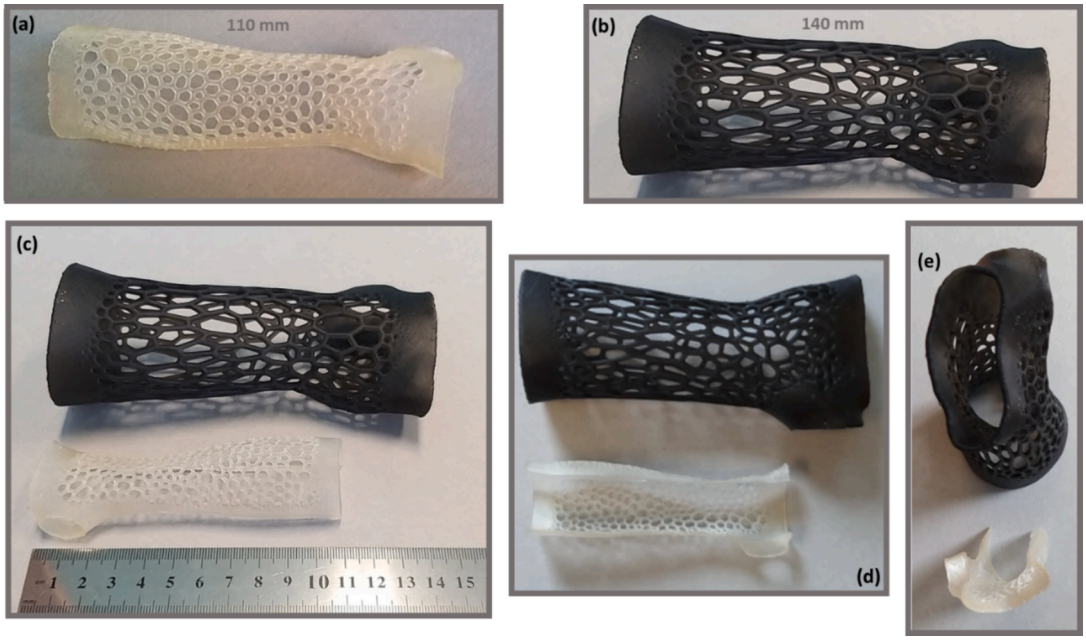

Fig. 11. 3D printed AESO-based objects unfilled (a) and filled (b) with 1 wt% of BC representing two different kinds of human forearm splints from different views (c), (d) and (e). (For interpretation of the references to colour in this figure legend, the reader is referred to the web version of this article.)

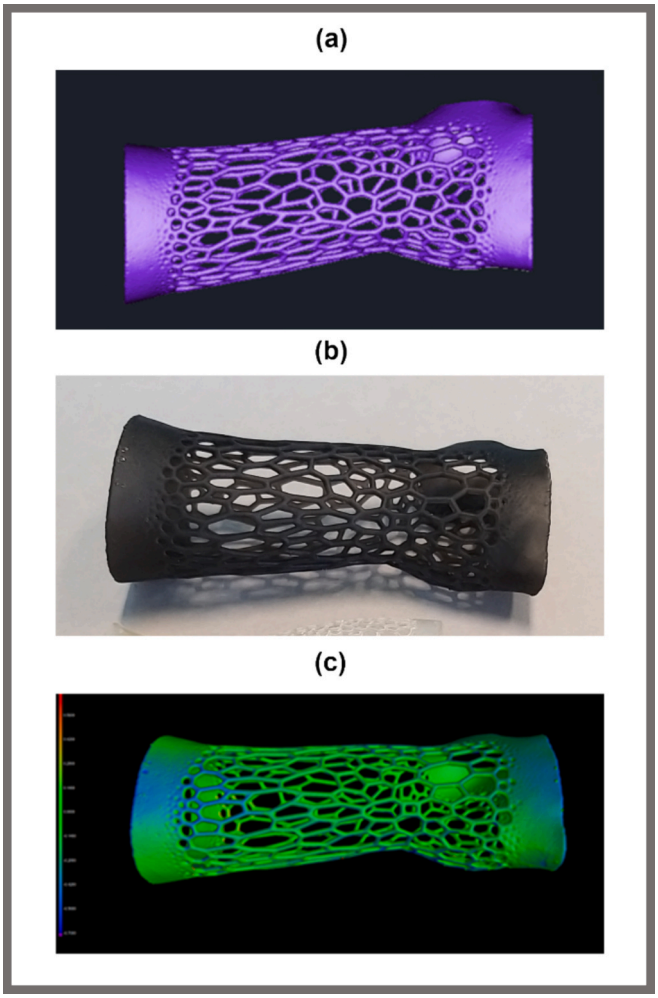

Fig. 12. CAD model (a), real geometry (b) and colored map (c) of the AESO-based object realized via LCD representing the forearm splint. (For interpretation of the references to colour in this figure legend, the reader is referred to the web version of this article.)

micro-CT scanning. The scan was aligned to the original CAD model via the best-fit registration function in VG Studio software, which ensures a precise overlay for comparison. Following alignment, deviations between the nominal design and the complex 3D printed geometry were calculated, as visible in Fig. 12(a) and Fig. 12(b), respectively. The results are clearly visible in Fig. 12(c), as a chromatic representation providing a visual and quantitative understanding of the accuracy of the selected printed part.

The creation of a coloured map for the analysis of the printing deviations is an easy way to have direct graphical feedback of the quality and accuracy of the printed part with respect to the original CAD model (Fig. 12a). The coloured map shows an almost entirely green-coloured deviation map, as reported in Fig. 12(c), confirming a high level of accuracy and consistency of the real printed piece of Fig. 12(b). This visual confirmation also evidences minimal deviations between the printed part and the scanned reference model. In fact, more than the 95 % of the printed object perfectly fits with the reference CAD model with a deviation less of 0.365 mm. Minor discrepancies can be ascribed to the resolution limits of the LCD printing process that can give rise to potential distortions. However, the overall green map for the printed part very challenging to realize via LCD supports the conclusion that the 3D printed forearm splint prototype closely reproduces the expected complex geometry showing high resolution and dimensional accuracy.

4. Conclusions

The work focused on the exploration of new photopolymer formulations consisting of bio-based materials, demonstrating their potential use in 3D printing via LCD technology. This approach is more cost-effective than other VP technologies achieving excellent results in terms of final resolution and printing speed.

The formulations printability via LCD was first studied by identifying the best printing parameters to optimize the printing process considering their viscosity under the selected curing conditions.

Several 3D printed parts with increasing complex architectures were realized by using LCD as VP technology by dispersing BC up to 2 wt% within an AESO photocurable resin to develop novel bio-based composites.

Thermal analyses, performed by TGA, viscoelastic properties by DMA, and tensile testing were carried out to study the BC-based composites behaviour.

Investigations into the characteristics of the printed samples revealed that the incorporation of BC at concentrations up to 1 wt% led to a good dispersion of the BC within the AESO-IBOMA matrix, thereby enhancing the rigidity of the resulting bio-based composites materials. However, higher concentrations, such as 2 wt% of filler, exhibited negative effects, surely due to the formation of BC clusters within the photocured network, as highlighted by FESEM, contributing to increase the material fragility, as also confirmed by tensile tests.

The results also revealed that the photocuring process within the LCD 3D printer does not have significant effects on the thermal properties of the composites in the presence of increasing amount of BC. However, the addition of the filler leads to a significant increase of the mechanical properties up to 1 wt% of BC.

Cell viability and cytocompatibility tests were also conducted on the unfilled and BC-based composites to evaluate their possible applications into the biomedical field. The results obtained evidence that the presence of BC does not influence the cell viability and cytocompatibility of the printed systems.

The choice of 1 wt% as the best BC concentration for the preparation of the AESO-based composites is based on a careful evaluation of multiple key factors resulting from the different characterization techniques. At this concentration, the material achieves an ideal balance between printability, mechanical performance, and biocompatibility. Higher concentrations lead to difficulties in processing due to the presence of clusters of BC particles that reduce the flowability within the vat. Moreover, in the presence of higher amount of BC, its tendence to absorb the UV radiation negatively affects the curing process and the layer adhesion, compromising the final printability. Furthermore, concentrations higher than 1 wt% result in insufficient mechanical performance of the specimens. Conversely, the AESO-based samples filled with BC at 1 wt% maintain a good level of mechanical properties and reveal good biocompatibility, ensuring that the final printed parts are safe for biomedical applications. Thus, 1 wt% represents the optimal compromise, providing a material with suitable properties for reliable printing, adequate mechanical properties, and safe interaction with biological systems.

As a result, two different prototypes for biomedical applications were successfully 3D printed using the formulation which has given the best results (with 1 wt% of BC), such as sustainable alternatives to the classical forearm splints. The prototypes realized via LCD show very high level of complexity and dimensional accuracy, as also confirmed by the green colored map coming from the micro-CT scan measurement, which suggests an almost complete consistency of the real printed piece with the CAD model. These findings represent an advance in the development of innovative solutions capable of meeting performance requirements and more sustainable manufacturing technologies. This can open the way to the adoption of these innovative composite materials in the biomedical sector by using LCD as useful 3D printing technology, contributing to the creation of eco-friendly products by reducing the

environmental impact.

Compliance with ethical standards

The authors also declare no known conflict of interest or personal relationships that could influence the present research work.

CRediT authorship contribution statement

Giovanna Colucci: Writing – review & editing, Writing – original draft, Visualization, Validation, Supervision, Methodology, Investigation, Formal analysis, Data curation, Conceptualization. **Federica Di Stefano:** Writing – original draft, Investigation, Formal analysis, Data curation. **Francesca Sacchi:** Writing – original draft, Methodology, Investigation, Formal analysis, Data curation. **Michela Licciardello:** Writing – original draft, Investigation, Formal analysis, Data curation. **Chiara Tonda-Turo:** Writing – review & editing, Supervision, Resources. **Luca Lavagna:** Writing – review & editing, Writing – original draft, Validation, Formal analysis. **Massimo Messori:** Writing – review & editing, Supervision, Resources, Project administration, Funding acquisition.

Ethics approval and consent to participate

The manuscript is approved by all authors for publication. I would like to declare on behalf of my co-authors that the work described is original research that has not been published previously, and not under consideration for publication elsewhere.

Funding

The present work was financially supported by MICS (Made in Italy – Circular and Sustainable) Extended Partnership and the European Union Next-Generation EU (PIANO NAZIONALE DI RIPRESA E RESILIENZA (PNRR) – MISSIONE 4 COMPONENTE 2, INVESTIMENTO 1.3 – D.D. 1551.11-10-2022, PE00000004). The paper reports only the authors' viewpoints, neither the European Union nor the European Commission are responsible for them.

Declaration of competing interest

The authors declare that they have no known competing financial interests or personal relationships that could have appeared to influence the work reported in this paper.

Acknowledgements

The authors would like to thank Mattia Bartoli and Alberto Giubilini from Politecnico di Torino for the kind supply of the BC powder and for micro-CT scanning, respectively.

Data availability

Data will be made available on request.

References

[1] Gustavsson J, Cederberg C, Sonesson U. Global food losses and food waste: extent, causes and prevention; study conducted for the International Congress Save Food! At Interpack 2011, [16 - 17 may], Düsseldorf, Germany. Rome: Food and Agriculture Organization of the United Nations; 2011.
[2] Bergeron FC. Energy and climate impact assessment of waste wood recovery in Switzerland. Biomass Bioenergy 2016;94:245–57. https://doi.org/10.1016/j.biombioe.2016.09.009.
[3] Lopatina A, Anugwom I, Blot H, Sánchez Conde Á, Mänttäri M, Kallioinen M. Re-use of waste cotton textile as an ultrafiltration membrane. J Environ Chem Eng 2021;9:105705. https://doi.org/10.1016/j.jece.2021.105705.
[4] Luque R, Campelo JM, Clark JH. 1 - Introduction: an overview of biofuels and production technologies. In: Luque R, Campelo J, Clark J, editors. Handb Biofuels Prod. Woodhead Publishing; 2011. p. 3–12. doi: 10.1533/9780857090492.1.3.
[5] Tamborrino V, Costamagna G, Bartoli M, Rovere M, Jagdale P, Lavagna L, et al. Catalytic oxidative desulphurization of pyrolytic oils to fuels over different waste derived carbon-based catalysts. Fuel 2021;296:120693. https://doi.org/10.1016/j.fuel.2021.120693.
[6] Basu P. Chapter 1 - Introduction. In: Basu P, editor. Biomass Gasif Pyrolysis Torrefaction. 3rd Ed. Academic Press; 2018. p. 1–27. doi: 10.1016/B978-0-12-812992-0.00001-7.
[7] Cha JS, Park SH, Jung S-C, Ryu C, Jeon J-K, Shin M-C, et al. Production and utilization of biochar: a review. J Ind Eng Chem 2016;40:1–15. https://doi.org/10.1016/j.jiec.2016.06.002.
[8] Pudełko A, Postawa P, Stachowiak T, Malińska K, Dróżdż D. Waste derived biochar as an alternative filler in biocomposites - mechanical, thermal and morphological properties of biochar added biocomposites. J Clean Prod 2021;278:123850. https://doi.org/10.1016/j.jclepro.2020.123850.
[9] Scavuzzo S, Zecchi S, Cristoforo G, Rosso C, Torsello D, Ghigo G, et al. Miscanthus-derived biochar as a platform for the production of fillers for the improvement of mechanical and electromagnetic properties of epoxy composites. C 2024;10. https://doi.org/10.3390/c10030081.
[10] Bartoli M, Arrigo R, Malucelli G, Tagliaferro A, Duraccio D. Recent advances in biochar polymer composites. Polymers 2022;14. https://doi.org/10.3390/polym14122506.
[11] Bifulco A, Bartoli M, Climaco I, Franchino MC, Battegazzore D, Mensah RA, et al. Coffee waste-derived biochar as a flame retardant for epoxy nanocomposites. Sustain Mater Technol 2024;41:e01079. https://doi.org/10.1016/j.susmat.2024.e01079.
[12] Torsello D, Ghigo G, Giorcelli M, Bartoli M, Rovere M, Tagliaferro A. Tuning the microwave electromagnetic properties of biochar-based composites by annealing. Carbon Trends 2021;4:100062. https://doi.org/10.1016/j.cartre.2021.100062.
[13] Bartoli M, Torsello D, Piatti E, Giorcelli M, Sparavigna AC, Rovere M, et al. Pressure-responsive conductive poly(vinyl alcohol) composites containing waste cotton fibers biochar. Micromachines 2022;13. https://doi.org/10.3390/mi13010125.
[14] Weber K, Quicker P. Properties of biochar. Fuel 2018;217:240–61. https://doi.org/10.1016/j.fuel.2017.12.054.
[15] Tengku Yasim-Anuar TA, Yee-Foong LN, Lawal AA, Ahmad Farid MA, Mohd Yusuf MZ, Hassan MA, et al. Emerging application of biochar as a renewable and superior filler in polymer composites. RSC Adv 2022;12:13938–49. https://doi.org/10.1039/D2RA01897G.
[16] Bélanger N, Prasher S, Dumont M-J. Tailoring biochar production for use as a reinforcing bio-based filler in rubber composites: a review. Polym-Plast Technol Mater 2023;62:54–75. https://doi.org/10.1080/25740881.2022.2089584.
[17] Baniasadi H, Lizundia E, Paganelli Z, Dammann N, Välinen L, Seppälä J, et al. Structure-property correlations study in biochar-enhanced polyamide composites for sustainable materials development. Compos B Eng 2024;286:111809. https://doi.org/10.1016/j.compositesb.2024.111809.
[18] Idrees M, Jeelani S, Rangari V. Three-dimensional-printed sustainable biochar-recycled PET composites. ACS Sustain Chem Eng 2018;6:13940–8. https://doi.org/10.1021/acssuschemeng.8b02283.
[19] Vidakis N, Kalderis D, Petousis M, Maravelakis E, Mountakis N, Bolanakis N, et al. Biochar filler in MEX and VPP additive manufacturing: characterization and reinforcement effects in polylactic acid and standard grade resin matrices. Biochar 2023;5:39. https://doi.org/10.1007/s42773-023-00238-6.
[20] Jandyal A, Chaturvedi I, Wazir I, Raina A, Ul Haq MI. 3D printing – a review of processes, materials and applications in industry 4.0. Sustain Oper Comput 2022;3:33–42. https://doi.org/10.1016/j.susoc.2021.09.004.
[21] Quan H, Zhang T, Xu H, Luo S, Nie J, Zhu X. Photo-curing 3D printing technique and its challenges. Bioact Mater 2020;5:110–5. https://doi.org/10.1016/j.bioactmat.2019.12.003.
[22] Sanchez-Rexach E, Johnston TG, Jehanno C, Sardon H, Nelson A. Sustainable materials and chemical processes for additive manufacturing. Chem Mater 2020;32:7105–19. https://doi.org/10.1021/acs.chemmater.0c02008.
[23] Voet VSD, Guit J, Loos K. Sustainable photopolymers in 3D printing: a review on biobased, biodegradable, and recyclable alternatives. Macromol Rapid Commun 2021;42:2000475. https://doi.org/10.1002/marc.202000475.
[24] Colucci G, Sacchi F, Bondioli F, Messori M. Fully bio-based polymer composites: preparation, characterization, and LCD 3D printing. Polymers 2024;16. https://doi.org/10.3390/polym16091272.
[25] Zhang Y, Xu Y, Simon-Masseron A, Lalevée J. Radical photoinitiation with LEDs and applications in the 3D printing of composites. Chem Soc Rev 2021;50:3824–41. https://doi.org/10.1039/D0CS01411G.
[26] Medellin A, Du W, Miao G, Zou J, Pei Z, Ma C. Vat Photopolymerization 3D printing of nanocomposites: a literature review. J Micro Nano-Manuf 2019;7. https://doi.org/10.1115/1.4044288.
[27] Al Rashid A, Ahmed W, Khalid MY, Koç M. Vat photopolymerization of polymers and polymer composites: processes and applications. Addit Manuf 2021;47:102279. https://doi.org/10.1016/j.addma.2021.102279.
[28] Tosto C, Saitta L, Latteri A, Blanco I. Development of recyclable bio-based epoxy/acrylate blends for liquid crystal display 3D printing. J Therm Anal Calorim 2024. https://doi.org/10.1007/s10973-024-13094-8.
[29] Pezzana L, Wolff R, Stampfl J, Liska R, Sangermano M. High temperature vat photopolymerization 3D printing of fully bio-based composites: green vegetable oil epoxy matrix & bio-derived filler powder. Addit Manuf 2024;79:103929. https://doi.org/10.1016/j.addma.2023.103929.

[30] Porcarello M, Mendes-Felipe C, Lanceros-Mendez S, Sangermano M. Design of acrylated epoxidized soybean oil biobased photo-curable formulations for 3D printing. Sustain Mater Technol 2024;40:e00927. https://doi.org/10.1016/j.susmat.2024.e00927.
[31] Auclair N, Kaboorani A, Riedl B, Landry V. Acrylated betulin as a comonomer for bio-based coatings. Part I: characterization, photo-polymerization behavior and thermal stability. Ind Crops Prod 2015;76:530–7. https://doi.org/10.1016/j.indcrop.2015.07.020.
[32] Lai H, Le Dot M, Chen J, Zhang J, Xiao P. Biomass-derived photoresins for digital light processing 3D printing of degradable objects. ACS Sustain Resour Manag 2025. https://doi.org/10.1021/acssusresmgt.5c00094.
[33] Liang B, Chen J, Guo X, Yang Z, Yuan T. Bio-based organic-inorganic hybrid UV-curable hydrophobic coating prepared from epoxidized vegetable oils. Ind Crop Prod 2021;163:113331. https://doi.org/10.1016/j.indcrop.2021.113331.
[34] Varganici C-D, Rosu L, Rosu D, Asandulesa M. From fossil to bio-based AESO–TiO2 microcomposite for engineering applications. Polymers 2024;16. https://doi.org/10.3390/polym16233363.
[35] Petousis M, Maravelakis E, Kalderis D, Saltas V, Mountakis N, Spiridaki M, et al. Biochar for sustainable additive manufacturing: thermal, mechanical, electrical, and rheological responses of polypropylene-biochar composites. Biomass Bioenergy 2024;186:107272. https://doi.org/10.1016/j.biombioe.2024.107272.
[36] Noè C, Cosola A, Tonda-Turo C, Sesana R, Delprete C, Chiappone A, et al. DLP-printable fully biobased soybean oil composites. Polymer 2022;247:124779. https://doi.org/10.1016/j.polymer.2022.124779.
[37] Navaruckiene A, Skliutas E, Kasetaite S, Rekštytė S, Raudoniene V, Bridziuviene D, et al. Vanillin acrylate-based resins for optical 3D printing. Polymers 2020;12. https://doi.org/10.3390/polym12020397.
[38] Lebedevaite M, Gineika A, Talacka V, Baltakys K, Ostrauskaite J. Development and optical 3D printing of acrylated epoxidized soybean oil-based composites with functionalized calcium silicate hydrate filler derived from aluminium fluoride production waste. Compos Part Appl Sci Manuf 2022;157:106929. https://doi.org/10.1016/j.compositesa.2022.106929.
[39] Chen J, Liu H, Zhang W, Lv L, Liu Z. Thermosets resins prepared from soybean oil and lignin derivatives with high biocontent, superior thermal properties, and biodegradability. J Appl Polym Sci 2020;137:48827. https://doi.org/10.1002/app.48827.
[40] Calovi M, Rossi S. Functional olive pit powders: the role of the bio-based filler in reducing the water uptake phenomena of the waterborne paint. Coatings 2023;13. https://doi.org/10.3390/coatings13020442.
[41] Arora N, Dua S, Singh VK, Singh SK, Senthilkumar T. A comprehensive review on fillers and mechanical properties of 3D printed polymer composites. Mater Today Commun 2024;40:109617. https://doi.org/10.1016/j.mtcomm.2024.109617.
[42] Zhou Z, Xu K, Li C, Lin J, Bian J, Sun K, et al. Assembly of 3D printed N-doped biochar as impeller with CaCO3 as sacrificial pore generator for enhanced dye adsorption. Chem Eng J 2024;497:154661. https://doi.org/10.1016/j.cej.2024.154661.
[43] Anerao P, Kulkarni A, Munde Y, Shinde A, Das O. Biochar reinforced PLA composite for fused deposition modelling (FDM): a parametric study on mechanical performance. Compos Part C Open Access 2023;12:100406. https://doi.org/10.1016/j.jcomc.2023.100406.
[44] Feliz Florian G, Ragoubi M, Leblanc N, Taouk B, Abdelouahed L. Biochar production and its potential application for biocomposite materials: a comprehensive review. J Compos Sci 2024;8. https://doi.org/10.3390/jcs8060220.
[45] Lastovickova DN, Toulan FR, Mitchell JR, VanOosten D, Clay AM, Stanzione III JF, et al. Resin, cure, and polymer properties of photopolymerizable resins containing bio-derived isosorbide. J Appl Polym Sci 2021;138:app50574. https://doi.org/10.1002/app.50574.
[46] Chen S, Zhang Q, Yang Z, Bian Y, Chen G, Li D, et al. Fabrication and characterization of light-curing soybean oil-based epoxy resin applied for LCD additive manufacturing. Ind Crop Prod 2023;202:117037. https://doi.org/10.1016/j.indcrop.2023.117037.
[47] Wu Y, Li C, Chen T, Qiu R, Liu W. Photo-curing 3D printing of micro-scale bamboo fibers reinforced palm oil-based thermosets composites. Compos Part Appl Sci Manuf 2022;152:106676. https://doi.org/10.1016/j.compositesa.2021.106676.
[48] Kousaalya AB, Ayalew B, Pilla S. Photopolymerization of acrylated epoxidized soybean oil: a photocalorimetry-based kinetic study. ACS Omega 2019;4:21799–808. https://doi.org/10.1021/acsomega.9b02680.
[49] Pezzana L, Emanuele A, Sesana R, Delprete C, Malmström E, Johansson M, et al. Cationic UV-curing of isosorbide-based epoxy coating reinforced with macadamia nut shell powder. Prog Org Coat 2023;185:107949. https://doi.org/10.1016/j.porgcoat.2023.107949.
[50] Colucci G, Aluigi A, Tonin C, Bongiovanni R. Photopolymerization of keratin-based thiol-ene coatings. Prog Org Coat 2014;77:1104–10. https://doi.org/10.1016/j.porgcoat.2014.03.009.
[51] Pezzana L, Melilli G, Guigo N, Sbirrazzuoli N, Sangermano M. Cationic UV curing of bioderived epoxy furan-based coatings: tailoring the final properties by in situ formation of hybrid network and addition of monofunctional monomer. ACS Sustain Chem Eng 2021;9:17403–12. https://doi.org/10.1021/acssuschemeng.1c06939.
[52] Bartoli M, Giorcelli M, Jagdale P, Rovere M, Tagliaferro A, Chae M, et al. Shape tunability of carbonized cellulose nanocrystals. SN Appl Sci 2019;1:1661. https://doi.org/10.1007/s42452-019-1727-2.
[53] Elkhalifa S, Parthasarathy P, Mackey HR, Al-Ansari T, Elhassan O, Mansour S, et al. Biochar development from thermal TGA studies of individual food waste vegetables and their blended systems. Biomass Convers Biorefinery 2022. https://doi.org/10.1007/s13399-022-02441-0.
[54] Sim M-Y, Park J-B, Kim D-Y, Kim H-Y, Park J-M. Dimensional accuracy and surface characteristics of complete-arch cast manufactured by six 3D printers. Heliyon 2024;10:e30996. https://doi.org/10.1016/j.heliyon.2024.e30996.
[55] Lebedevaite M, Talacka V, Ostrauskaite J. High biorenewable content acrylate photocurable resins for DLP 3D printing. J Appl Polym Sci 2021;138:50233. https://doi.org/10.1002/app.50233.
[56] Tonda-Turo C, Carmagnola I, Chiappone A, Feng Z, Ciardelli G, Hakkarainen M, et al. Photocurable chitosan as bioink for cellularized therapies towards personalized scaffold architecture. Bioprinting 2020;18:e00082. https://doi.org/10.1016/j.bprint.2020.e00082.
[57] Mo Y, Design JS. Simulation, and fabrication of composite lattice orthoses with enhanced structural performance. J Mech Des 2024;147. https://doi.org/10.1115/1.4066578.
[58] Blaya F, Pedro PS, Silva JL, D'Amato R, Heras ES, Juanes JA. Design of an orthopedic product by using additive manufacturing technology: the arm splint. J Med Syst 2018;42:54. https://doi.org/10.1007/s10916-018-0909-6.